Boundary Layers and Separation on a Spheroid at Incidence

V.C. Patel* and J.H. Baek†
The University of Iowa, Iowa City, Iowa

Three-dimensional boundary layers on a 6:1 spheroid at an incidence of 10 deg have been calculated at two Reynolds numbers. At the lower Reynolds number, the boundary layer is predominantly laminar, but at the higher Reynolds number it includes laminar, transitional, and turbulent-flow regions. Comparisons have been made with the previously existing data. The results clearly deomonstrate the capabilities and limitations of first-order boundary-layer theory.

I. Introduction

THE three-dimensional incompressible boundary layer on bodies of revolution has been the subject of many recent investigations. Among the experimental studies are those of Werle,[1] Wilson,[2] Peake et al.,[3] Han and Patel,[4] Ramaprian et al,[5] Hayashita,[6] and Meier et al.[7-10] Most of the early studies were restricted to flow visualization and, to date, much of the available information is concerned with flow at or close to the surface. Measurements within the boundary layer are quite limited.[5,6-8] On the other hand, there is an increasing number of numerical studies (see, e.g., Refs. 11-22) in which different methods are used to solve the boundary-layer equations for laminar as well as turbulent flows. These are of course able to generate much more information than can be extracted from even the most detailed experiments. In a few instances where the results of the calculations have been compared with experimental data (e.g., Refs 15,18,21,22), it is found that some of the observed features of the flow can be reproduced quite successfully, whereas others remain unexplained. In particular, experiments on bodies of revolution as well as other shapes indicate different types of flow separation resulting in a wide variety of flow patterns, whereas most calculations terminate at an ill-defined separation point or line. Frequently, separation is said to occur when the particular boundary-layer calculation method meets with some numerical irregularity or catastrophe. Thus, the problem of identifying the type and location of separation of a three-dimensional boundary layer by numerical means remains controversial. This paper attempts to address this issue by means of detailed comparisons between boundary-layer calculations and experimental data.

The calculation method employed here has been described previously[15,23] in some detail. For the present purposes, it suffices to note the major features. The method solves the usual thin boundary-layer equations in the body-fitted orthogonal coordinates shown in Fig. 1 using an ADI (alternating-direction-implicit) numerical scheme. The turbulence model is based on the turbulent kinetic-energy equation, a prescribed turbulence length-scale distribution, and the assumption that the directions of the stress and rate-of-strain vectors are coincident. The method is capable of calculating laminar as well as turbulent boundary layers, transition being simulated by "switching on" the turbulence model along a prescribed transition line. No attempt has been made to tailor the model constants or functions for better representation of the development of turbulence over a finite transition length. Finally, for turbulent as well as laminar flow, the equations are solved numerically up to the wall without using any wall functions.

In the following, we consider the flow over a prolate spheroid of axes ratio 6:1 which has been used in the detailed experimental investigations of Meier et al.[7-10] Furthermore, we shall confine our attention to a moderate incidence of 10 deg, since it has been explored in greatest detail. The experimental information is first reviewed to point out the most significant features. The results of the boundary-layer calculations are then presented and compared with the data.

II. Review of Experiments

In the experiments of Meier et al.,[7-10] a 6:1 prolate spheroid, 2.4 m long and 0.4 m maximum diameter, has been tested over a range of incidences and at two Reynolds numbers, namely $Re \equiv (U_\infty L/\nu) = 1.6\times10^6$ and 7.2×10^6, corresponding to the reference freestream velocities, $U_\infty = 10$ and 45 m/s. For the case $\alpha = 10$ deg, the available measurements include the distribution of the pressure coefficient $C_p = (p-p_\infty)/\frac{1}{2}\rho U_\infty^2$ and the magnitude and direction of the skin-friction vector $C_f = \tau_w/\frac{1}{2}\rho U_\infty^2$, at both Reynolds numbers. The longitudinal and circumferential components of mean velocity, U and W, respectively, in the notation of Fig. 1, were also measured across the boundary layer at two axial positions at the higher Reynolds number. Since a tripping device was not employed, the boundary layer is initially laminar, and transition, when present, occurs naturally.

The pressure distributions measured at the two Reynolds numbers are compared with that predicted by potential-flow theory in Fig. 2a and the corresponding longitudinal and circumferential pressure gradients are shown in Fig. 2b and 2c, respectively. These are defined as follows:

$$(\nabla C_p)_x = \frac{\partial(2C_p)}{h_1\partial(X/L)}, \qquad (\nabla C_p)_\theta = \frac{\partial(2C_p)}{h_3\partial\theta}$$

where $h_1 = \{1+(dr/dX)^2\}^{\frac{1}{2}}$, $h_3 = r/X$), and r is the transverse radius of the body. It should be noted that this is one of a few experiments in three-dimensional boundary-layer flows where the pressures have been measured at such closely spaced intervals in both directions that the gradients can be evaluated without much uncertainty.

Figure 2 indicates several interesting differences among the three pressure distributions. Over the windward side of the body the measured pressures resemble those in potential flow but are consistently higher. This may be due to a "negative blockage" usually encountered in an open-jet wind tunnel or to an uncertainty in the reference pressure. As shown in Figs. 2b and 2c, however, the influence of these differences on the pressure gradients that enter the boundary-layer equations are quite small up to $X/L = 0.65$.

Received July 15, 1983; revision received March 2, 1984.

*Professor of Mechanical Engineering and Research Engineer, Iowa Institute of Hydraulic Research. Member AIAA.

†Research Assistant, Iowa Institute of Hydraulic Research.

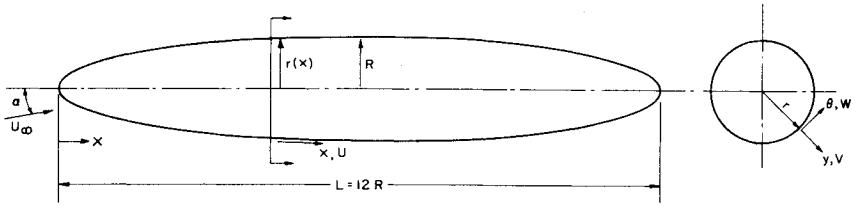

Fig. 1 Notation.

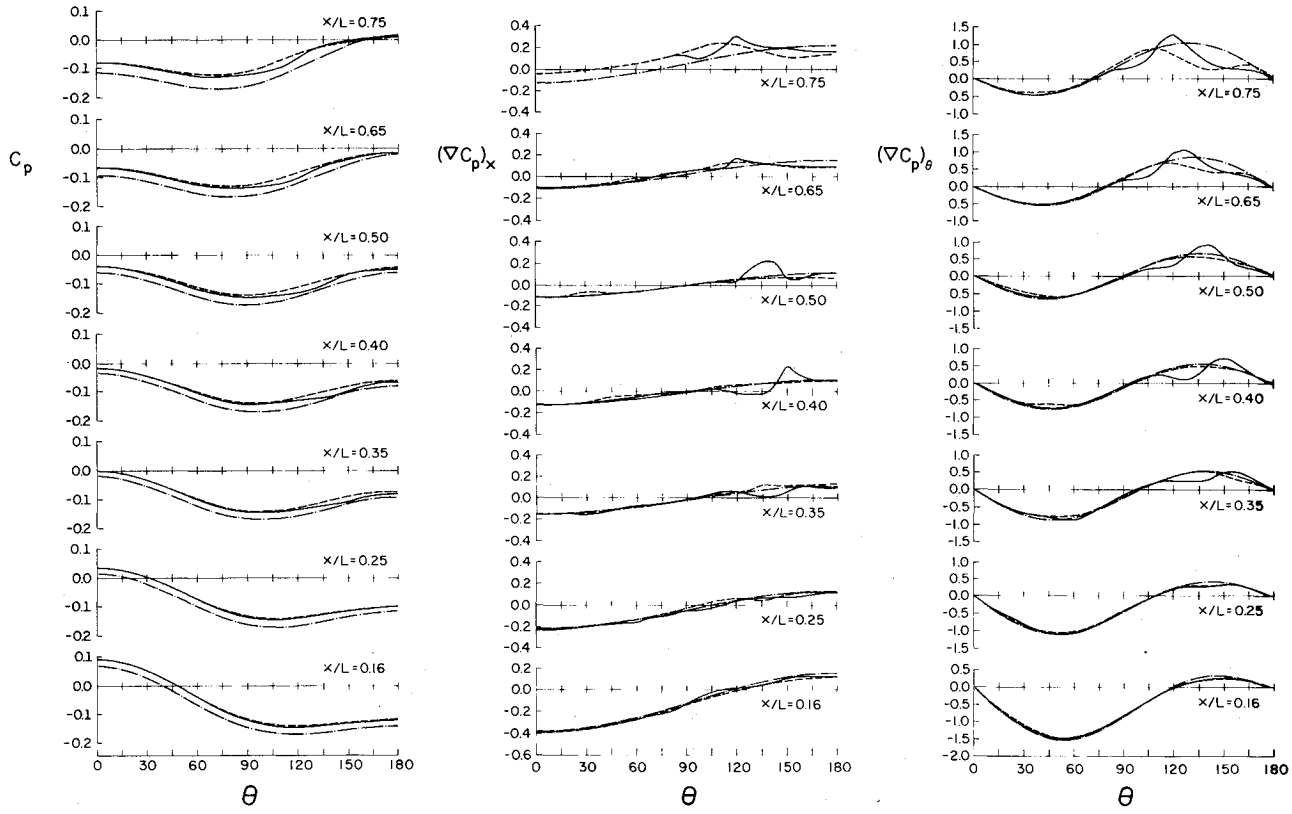

Fig. 2 Potential-flow and measured pressure distributions and gradients: – – – potential flow; —— $Re = 1.6 \times 10^6$, --- $Re = 7.2 \times 10^6$.

At the lower Reynolds number, the measured pressure distribution and gradients show marked departures from potential flow, starting at approximately $X/L = 0.25$ in the region 120 deg $< \theta <$ 150 deg, and spreading to 80 deg $< \theta <$ 180 deg by $X/L = 0.75$. The development of a short circumferential plateau of constant pressure at and beyond $X/L = 0.35$ is reflected in the positive (adverse) longitudinal and circumferential pressure gradients. The plateau is followed by a pressure rise toward the leeward side, and associated with this are somewhat larger pressure gradients than in potential flow,

At the higher Reynolds number, Fig. 2a shows that there is no constant-pressure plateau but a gradual reduction in the pressure coefficient on the leeward side, starting at $\theta = 180$ deg near $X/L = 0.40$ and spreading to 105 deg $< \theta <$ 180 deg by $X/L = 0.75$. Significant departures of the experimental pressure gradients from potential flow are also not evident until about $X/L = 0.65$.

The measured wall shear-stress vectors at the two Reynolds numbers shown in Figs. 3 and 4. At the lower Reynolds number (Fig. 3), we can distinguish a narrow region, starting at $\theta \sim 125$ deg at $X/L = 0.395$ and extending to $\theta \sim 90$ deg at $X/L = 0.825$, of rather small near-zero wall shear stress. Just beyond the near-zero stress region, in the circumferential direction, is a growing wedge of much larger stresses. This is believed to be due to transition to turbulent flow. The wedge grows from 140 deg $< \theta <$ 160 deg at $X/L = 0.395$ to 105 deg $< \theta <$ 180 deg at $X/L = 0.825$. The lower stresses along the leeward plane of symmetry ($\theta = 180$ deg) up to $X/L \sim 0.74$ indicate that the flow continues to be laminar over a diminishing region on the leeside up to that station.

The shear-stress measurements at the higher Reynolds number, shown in Fig. 4, are quite different, since the flow over a large part of the body is turbulent. The location of the zone of transition from laminar to turbulent flow can be inferred from the relative magnitudes of the stresses and is in accordance with the observations of Meier and Kreplin[7] on the basis of the surface hot-film signals. For later reference, the position of the transition line determined by Meier and Kreplin at this Reynolds number is shown in Fig. 5b. Finally, Fig. 4 indicates a zone of near-zero stress at $X/L = 0.936$, which is close to the sting used to support the model in the wind tunnel.

The foregoing review of the available experimental information indicates the complexities of the flows to be addressed computationally. It is clear that the two cases provide ample opportunities to explore the performance and limitations of three-dimensional boundary-layer calculation methods.

III. Numerical Solutions

The calculations were started just downstream of the axial position containing the potential-flow stagnation point, using the procedure described in Ref. 15. There were 21 grid points across the boundary layer. Some earlier solutions, reported in Ref. 22, were obtained with a circumferential step size $\Delta\theta = 15$ deg. The results to be presented here were obtained with a step size of 7.5 deg, primarily for better resolution of the flow in

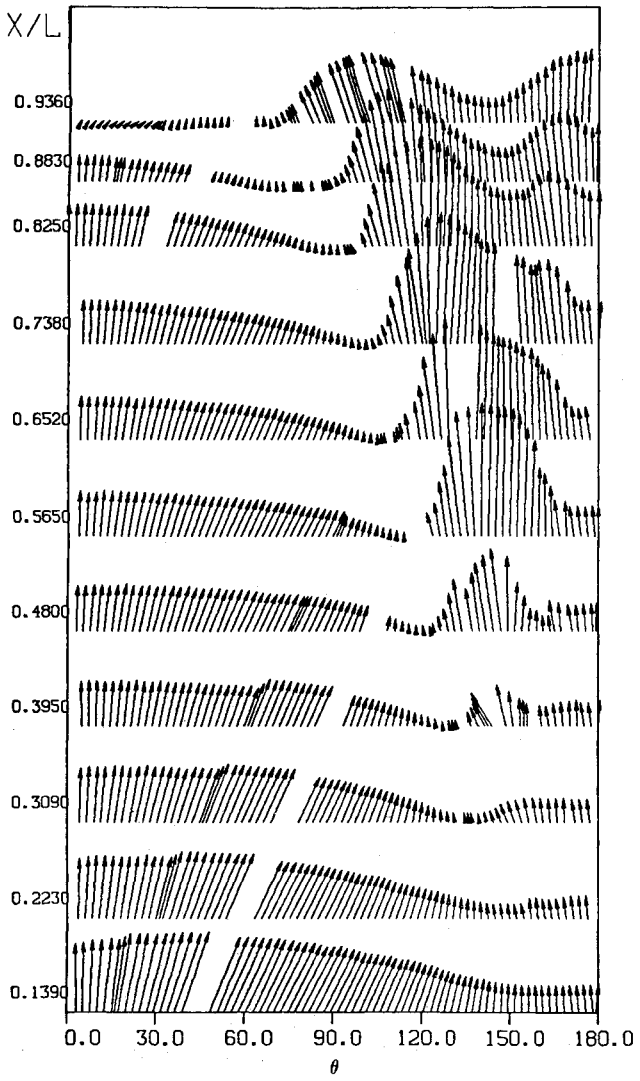

Fig. 3 Measured wall shear stress, $Re = 1.6 \times 10^6$.

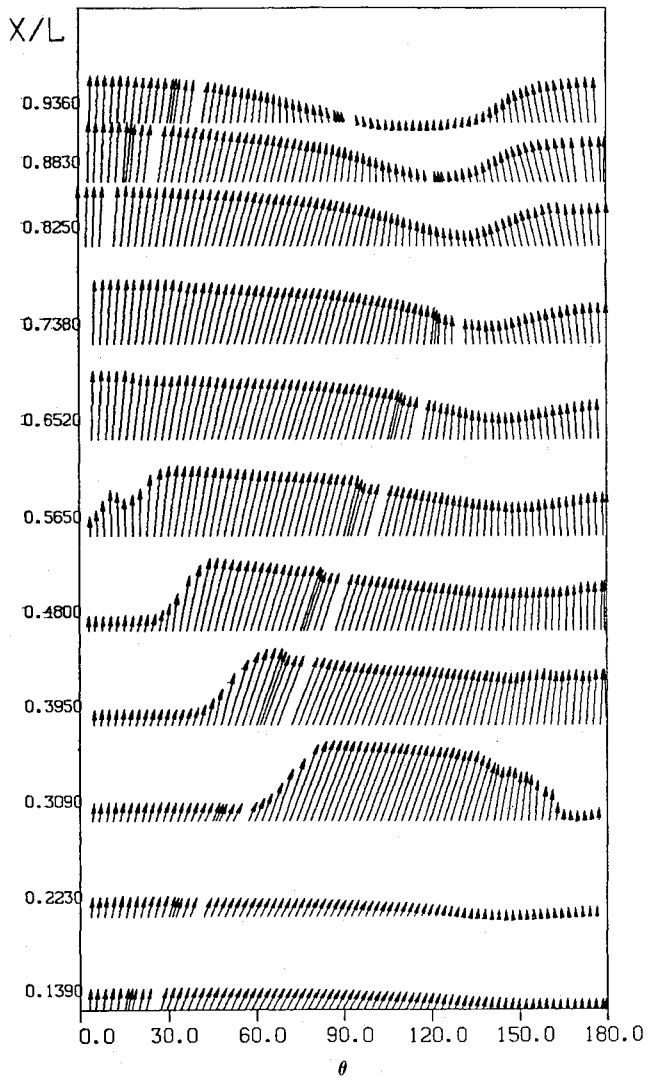

Fig. 4 Measured wall shear stress, $Re = 7.2 \times 10^6$.

certain key areas. Detailed comparisons between the two sets of calculations indicated grid dependence and lack of numerical convergence in regions where the magnitude of the wall shear stress became very small (typically $|C_f| < 0.0001$). Although we shall discuss the possible reasons for this, it should be emphasized that such regions have been excluded from the results presented in this section.

In view of the differences noted earlier between the potential-flow and experimental pressure distributions and pressure gradients, calculations have been performed using both. Since the experimental pressure distributions in the nose region indicated more scatter, the calculations in these cases were started at $X/L = 0.127$ using the solutions with the potential-flow pressures and scaling the velocity profiles for the difference between the measured and theoretical pressure coefficients. Note that the boundary layer is laminar at $X/L = 0.127$ at both Reynolds numbers. The subsequent solutions utilized the experimental pressures and gradients shown in Fig. 2.

A. $Re = 1.6 \times 10^6$

For this case, calculations were performed assuming laminar flow. Although these solutions were continued almost up to the tail of the body, we shall show the results primarily up to $X/L = 0.4$, since numerical problems were first encountered just downstream of this position over a wedge-shaped region on the body roughly coincident with a line

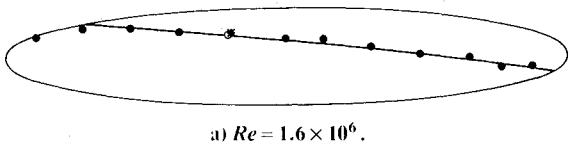

a) $Re = 1.6 \times 10^6$.

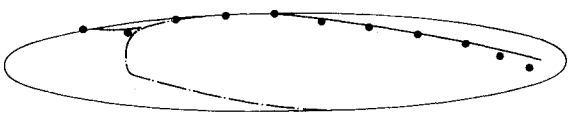

b) $Re = 7.2 \times 10^6$.

Fig. 5 Circumferential flow reversal lines. *, calculated zero stress point, •, experimental CFR:——, calculated CFR (potential-flow pressure distribution):— · —, experimental transition line.

along which the wall shear stress became very small and the leeward plane of symmetry.

The main results of the calculations, with potential-flow and measured pressure distributions, are shown in Figs. 5a, 6, and 7. To facilitate comparison with the experimental wall shear-stress data of Fig. 3, the same scales have been used in Fig. 6, and calculations are shown at axial locations corresponding to the measurement stations. Figure 7 shows the resultant of the circumferential (W) and normal (V) components of the velocity vector. For clarity, these profiles

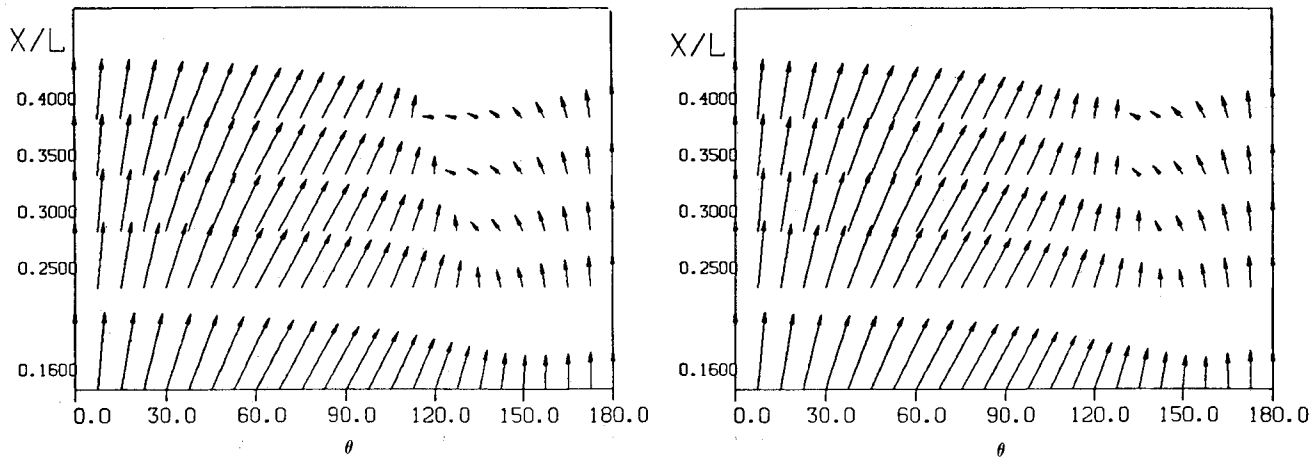

a) Potential-flow pressure distribution. b) Experimental pressure distribution.

Fig. 6 Calculated wall shear stress, $Re = 1.6 \times 10^6$.

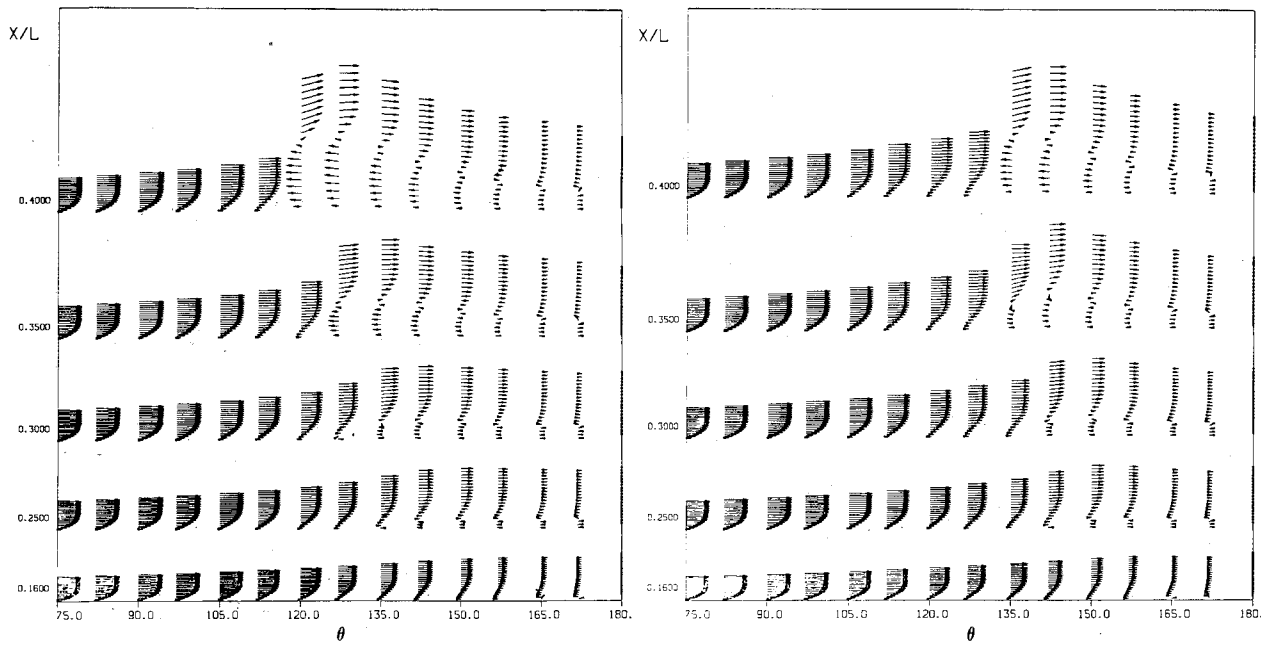

a) Potential-flow pressure distribution. b) Experimental pressure distribution.

Fig. 7 Velocity vectors in the y-θ plane, $Re = 1.6 \times 10^6$.

are shown only in the region $75 \leq \theta \leq 180$ deg, and the vertical scale has been expanded by a factor of five.

Figure 7 shows the development of a zone of circumferentially reversed flow starting on the leeward plane of symmetry just downstream of $X/L = 0.16$ and spreading outward from there until, at $X/L = 0.4$, it occupies 120 deg $< \theta <$ 180 deg in the calculations with potential-flow pressure distribution, and 135 deg $< \theta <$ 180 deg in those with the experimental pressure distribution. The boundary layer in this region is relatively thick. It is also possible to identify this region in Fig. 6 from the changes in the direction of the wall shear stress relative to the axis of the body, and to define a line on the body that demarcates circumferential flow reversal (CFR line). The experimental and calculated positions of this line are shown in Fig. 5a. Quite satisfactory agreement is observed in this respect, in spite of the numerical difficulties on the leeward side of this line. Note that such a line is "geometric" insofar as it is defined with respect to the geometry of the body and not that of the flow.

Calculations with both pressure distributions indicate that there exists a point at $X/L = 0.4$ ($\theta = 120$ deg and 135 deg in Figs. 6a and b, respectively) at which the direction of the wall shear stress changes abruptly and its magnitude becomes very small. Within the resolution of the numerical grid, this point coincides with almost explosive growth in boundary-layer thickness (see Fig. 7) and with the beginning of the numerical difficulties noted earlier.

A comparison between the solutions obtained with the two pressure distributions indicates that they are qualitatively similar. The major difference lies in the extent of the circumferential flow reversal zone and the location of the point of minimum wall shear stress and abrupt changes in its direction. Both occur closer to the leeward plane of symmetry with the experimental pressure distribution.

Finally, a comparison can be made between the wall shear-stress calculations shown in Fig. 6 and the corresponding experimental data of Fig. 3. The following observations can be made:

1) In the laminar flow up to $X/L = 0.3$, the calculations with potential-flow pressure distribution agree well with the data with respect to both magnitude and direction (see also Fig. 11), except in a small region around the CFR line where the predicted stresses are larger.

2) As may be expected from the relief of the measured pressure gradients in this region, the use of the experimental pressure distribution leads to even higher stresses and therefore somewhat poorer agreement with the data.

3) Beyond $X/L = 0.3$, the two calculations agree over a large region ($\theta < 100$ deg) on the windward side of the body with the measured stress directions, but the predicted magnitudes are higher. However, the corresponding data indicate some irregularities in magnitude.

4) At $X/L = 0.4$, the experiments indicate transition just beyond the stress minimum and the CFR line. In this region both calculations predict very small stresses. However, the accompanying abrupt changes in the direction of the wall shear stress are not observed in the experiment, due, presumably, to transition.

5) The point of minimum stress in the experiment is located at $\theta = 127$ deg, whereas the calculations with potential-flow and measured pressure distributions predict near-zero stress at $\theta = 122$ deg and 136 deg, respectively.

6) The calculated shear stress along the leeward plane of symmetry, $\theta = 180$ deg, continues to agree well with the data up to $X/L = 0.4$, indicating laminar flow along that line.

7) Figures 6, 7, and 2 show that the observed departures of the pressure distribution from potential flow are correlated with the zone of small wall shear and rapid boundary-layer growth.

B. $Re = 7.2 \times 10^6$

For this case, the laminar boundary-layer calculations were continued up to the experimentally observed transition line shown in Fig. 5b and the turbulence model was activated as this line was crossed along each meridian. Thus, for example, at $X/L = 0.3$ (see Figs. 4 and 5b), the computational domain includes laminar flow over the windward side, transitional and turbulent flow over the middle, and laminar flow again near the leeward plane of symmetry. The flow becomes turbulent over the entire circumference only beyond $X/L = 0.56$, where the transition line crosses the windward symmetry plane.

These calculations also indicated circumferential flow reversal in the upstream laminar boundary layer (Fig. 5b) but, due to transition to turbulent flow, numerical difficulties were

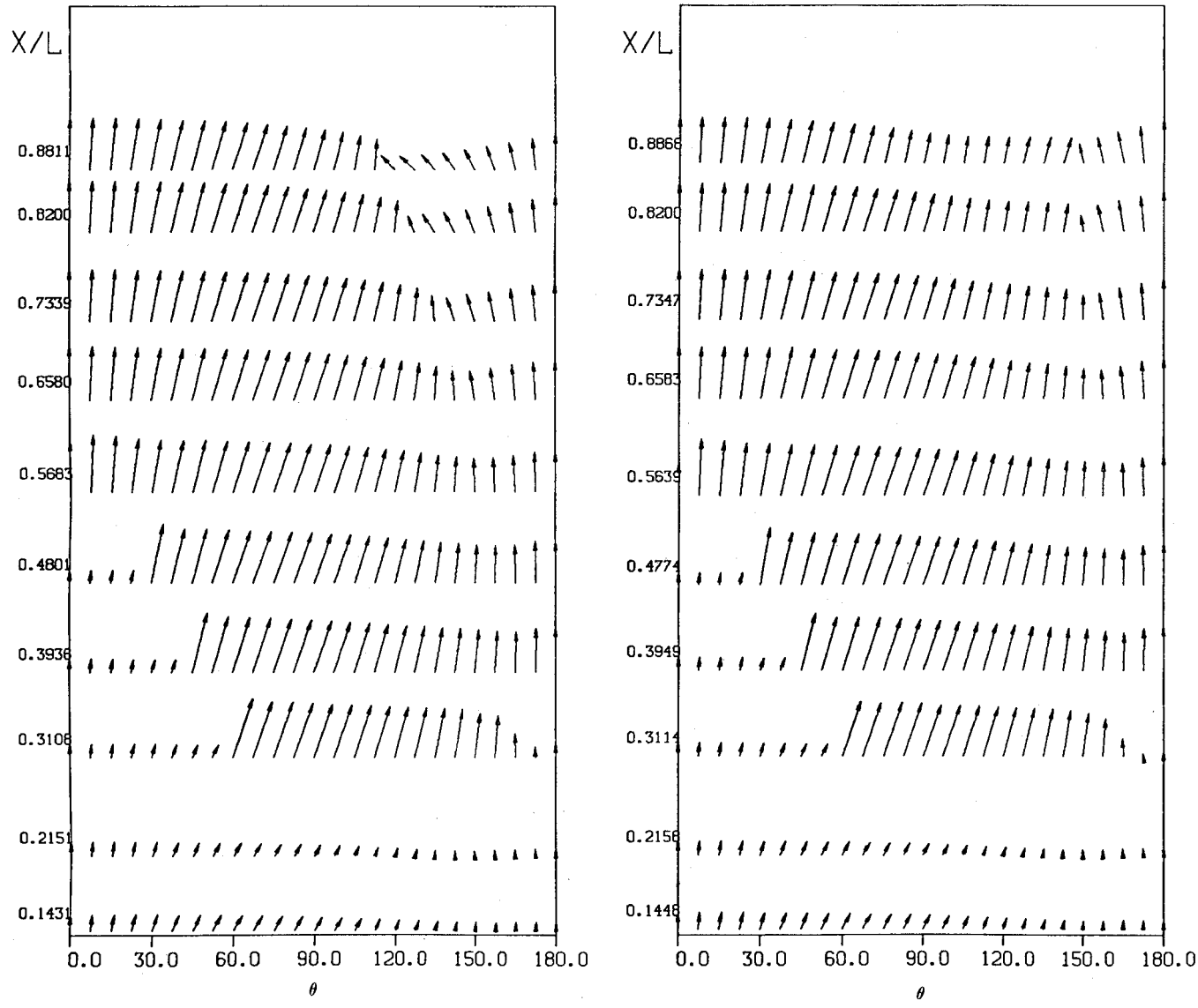

a) Potential-flow pressure distribution. b) Experimental pressure distribution.

Fig. 8 Calculated wall shear stress, $Re = 7.2 \times 10^6$.

not encountered at $X/L=0.4$ as in the previous case. The results of the calculations with the potential-flow and measured pressure distributions are shown in Fig. 5b and 8-10. As pointed out earlier in Fig. 2, the measured pressure gradients at this higher Reynolds number are in substantial agreement with those in potential flow over a large region on the windward side of the body. Consequently, the two sets of calculations are essentially the same in this region. The calculated wall shear-stress plots of Fig. 8, the cross-stream velocity vectors of Fig. 9, and the detailed axial and circumferential velocity-profiles of Fig. 10 indicate that significant differences between the results with potential-flow and measured pressure distributions are observed, as expected, on the leeward side. Also, as in the laminar case, the region of circumferential-flow reversal is smaller with the experimental pressure distribution.

Figure 5b shows a short CFR line in the laminar flow ahead of transition on the leeside. This is essentially the same as that calculated at the lower Reynolds number. It disappears after transition but a new CFR line is predicted in the turbulent flow further downstream. This line is of course closer to the leeside than the corresponding line in purely laminar flow, indicating the greater capability of turbulent flow to overcome the adverse circumferential pressure gradient before flow reversal. The experimentally observed CFR lines are again in good agreement with the calculations.

Comparison of Fig. 8 with Fig. 4 shows that the calculations reproduce the major features observed in the experiments except in the neighborhood of transition. The agreement in this region can be improved by incorporating a damping or intermittency function in the turbulence model in order to accomplish a more gradual change from laminar to turbulent flow. The calculated shear stresses in the turbulent flow just after transition tend to be lower than those measured. This again may be due to the inadequacy of the turbulence model for transitional flows. Further downstream, where the flow has recovered from transition, both calculations show good agreement with the data over a large portion of the body on the windward side and over a somewhat smaller region near the leeward plane of symmetry. However, substantial differences are observed in the region where the experimental data show a stress minimum, the calculated magnitudes being higher. Note that the data indicate almost zero stress at $X/L=0.883$, $\theta\sim 120$ deg and at $X/L=0.936$, 90 deg $<\theta<$ 130 deg, and the flow features are somewhat similar to those observed in the lower Reynolds number case. The present calculations indicated the first signs of numerical difficulties just beyond $X/L=0.88$.

The reasons for the poor performance of the calculations in the zone of the stress minimum are not entirely evident from the wall shear stresses. The cross-stream velocity vectors shown in Fig. 9 provide some explanation. It should be pointed out that, unlike the corresponding plot of Fig. 7 for laminar flow, the vertical and horizontal length scales are nearly the same in Fig. 9 and therefore it provides a true picture of the variation of the boundary-layer thickness in the circumferential direction. Thus, for example, at $X/L=0.75$, the ratio of the maximum boundary-layer thickness, which occurs at $\theta\sim 157.5$ deg, to the local body radius is approximately 0.67. The rapid thickening of the boundary layer and the development of a vortical flow on the leeside is associated with the convergence of near-wall streamlines from both sides. The thick boundary layer implies a strong viscous-inviscid interaction even in the absence of separation, and it is not surprising that the use of the measured surface pressure distribution does not guarantee improved agreement with experiment in all respects.

The detailed velocity-profile comparisons of Fig. 10 show that there is little to choose between the two sets of calculations except in the region of viscous-inviscid interaction. At $X/L=0.64$, the calculations are in good agreement with the data everywhere except in the zone 135 deg $<\theta<$ 165 deg, where Fig. 2 first shows substantial differences in the pressure gradients and where Fig. 9 indicates a thickening of the boundary layer. However, the measured boundary layer is thinner than that predicted by either calculation. The situation at $X/L=0.71$ is quite similar, but

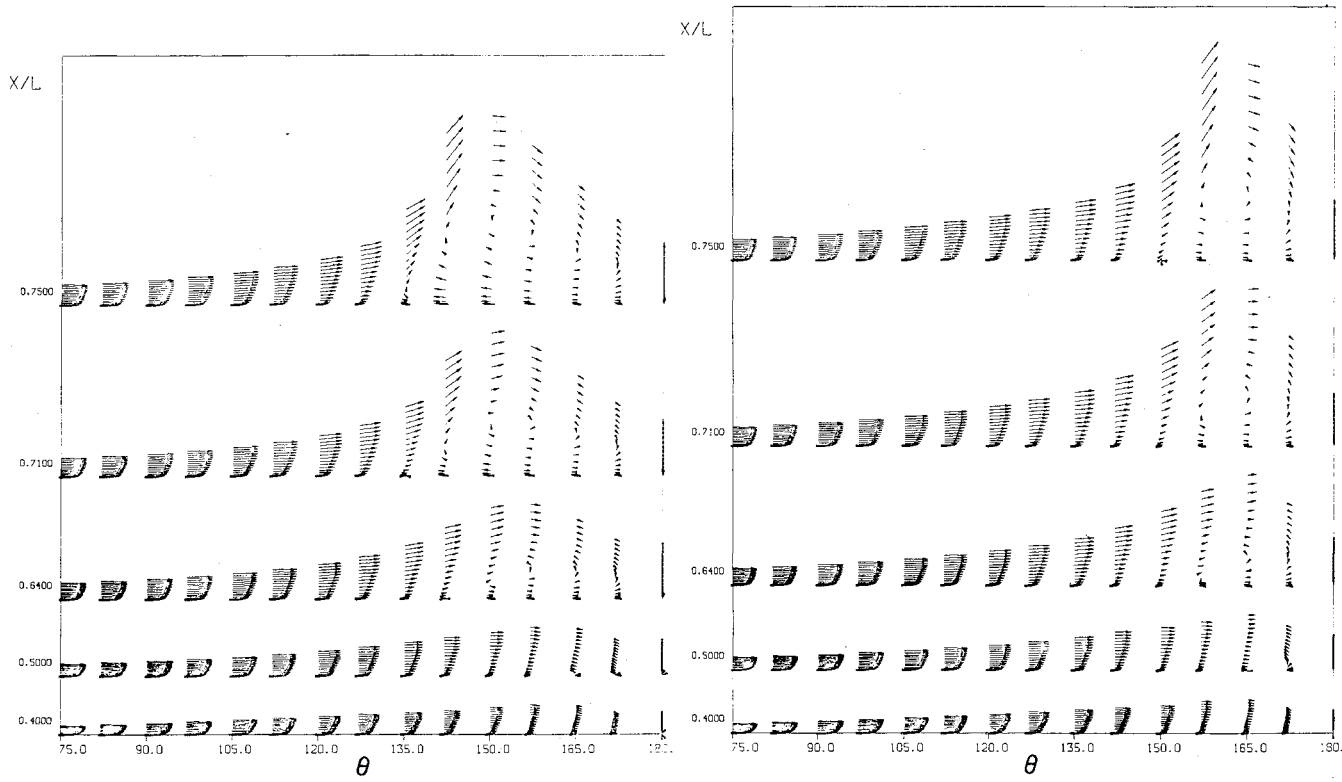

a) Potential-flow pressure distribution. b) Experimental pressure distribution.

Fig. 9 Velocity vectors in the y-θ plane, $Re=7.2\times 10^6$.

with one important difference: The measured velocity components at the edge of the boundary layer do not agree with those calculated with either the potential-flow or experimental pressure distribution over a circumferential extent much larger than that in which the boundary layer is thick. In other words, the measured velocities and directions in the external flow are not compatible with the pressure distribution measured at the surface. If systematic experimental errors of this magnitude are discounted, the differences imply not only a variation of pressure across the thick boundary layer but also significant changes in the direction of the external flow over regions quite remote from that where the boundary layer is thick. Thus, the thick boundary layer is responsible for a reorientation of the external flow over the entire circumference. The observed decrease in the measured transverse component of velocity on the windward side is compatible with this explanation.

Two other aspects of the calculations are also noteworthy. The first is that the boundary layer along the leeward plane of symmetry is predicted quite well, especially with the measured pressure distribution, almost up to $X/L=0.71$. Second, the calculated axial or primary component of the mean velocity in the wall region is in good agreement with measurements. These suggest that the turbulence model employed here is not a major source of the disagreements observed in the outer part of the boundary layer.

IV. Separation

We shall now explore the reasons for, and the implications of, the numerical problems encountered in the laminar boundary-layer calculations at the lower Reynolds number. Continuation of the present calculations downstream of $X/L=0.4$ showed grid-independent solutions over a diminishing domain on the windward side of the body, up to a line just to the leeside of the CFR line. As this line was approached, the magnitude of the wall shear stress became very small and its direction changed rapidly, the angle between the stress vector and the body axis changing from zero at the CFR line to values so large (~ 75 deg) that the wall cross-flow angle (i.e., the angle between the wall shear stress and the external flow) became 90 deg. (Note that this criterion is often invoked to pronounce separation, especially in integral calculation methods.) Also, the boundary layer thickened very rapidly and developed large values of the normal velocity component (Fig. 7). Solution features similar to those noted above have also been observed in previous calculations (see, e.g., Wang,[12, 13] Patel and Choi,[15] Cebeci et al., [18] and Ragab[21] and have been used to infer the imminence or occurrence of separation.

It is generally agreed that the flow on the windward side, at least up to the CFR line, can be calculated with some confidence using a variety of numerical schemes since there is no difficulty in identifying the corresponding zone of dependence for this region. It is also acknowledged that the behavior of the solutions in the neighborhood of the CFR line is related in some way to the imminence of separation. Another point of agreement is that the convergence of skin-friction lines, or the limiting streamlines at the wall, from both sides is a symptom of separation. However, there is little consensus among researchers on the precise definition of separation or the shape of the separation line.

Figure 11 shows the magnitude of the wall shear stress according to present calculations with the potential-flow pressure distribution. This is the same information as in Fig. 4a, except that typical solutions beyond $X/L=0.4$ have been added and it is now possible to make a direct comparison with

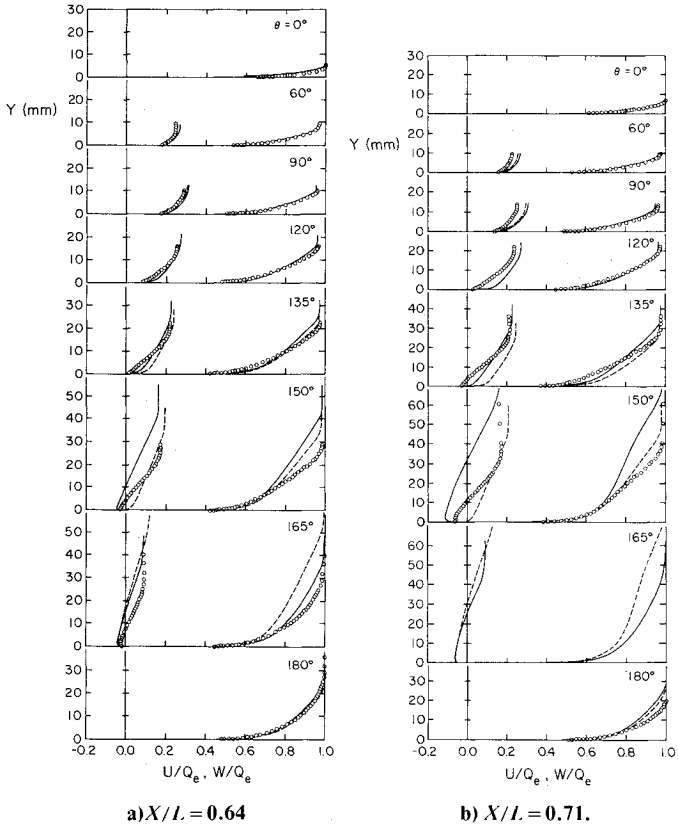

a) $X/L=0.64$ b) $X/L=0.71$.

Fig. 10. Axial and circumferential velocity profiles, $Re=7.2\times10^6$. – – – potential flow pressure, —measured presssure, ○ experiment.

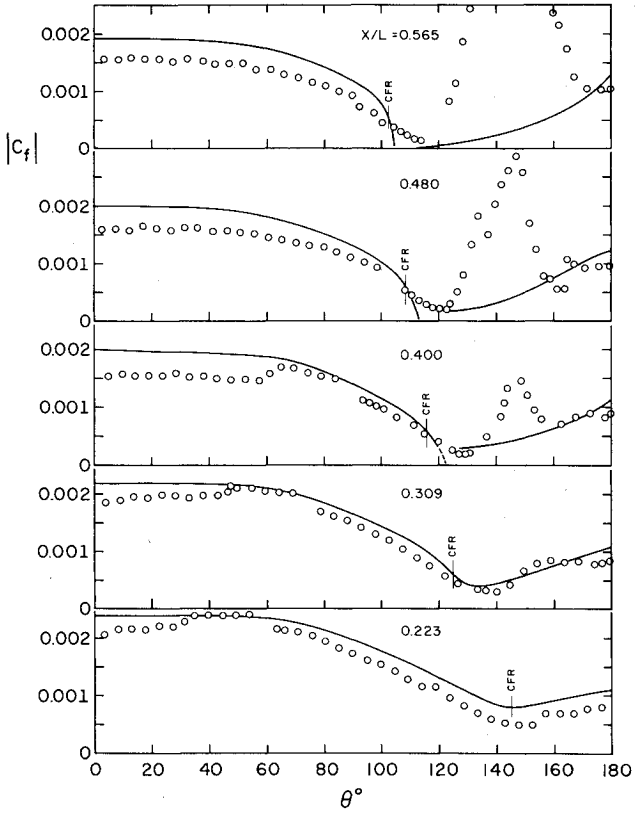

Fig. 11 Wall shear-stress magnitude, $Re=1.6\times10^6$ ○ experiment, – – –calculation.

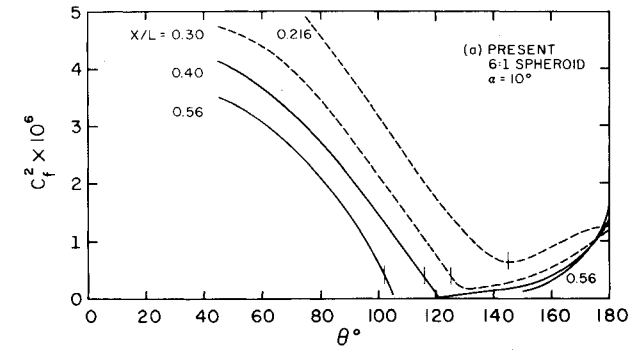

a) Present 6:1 spheroid, $\alpha = 10$ deg.

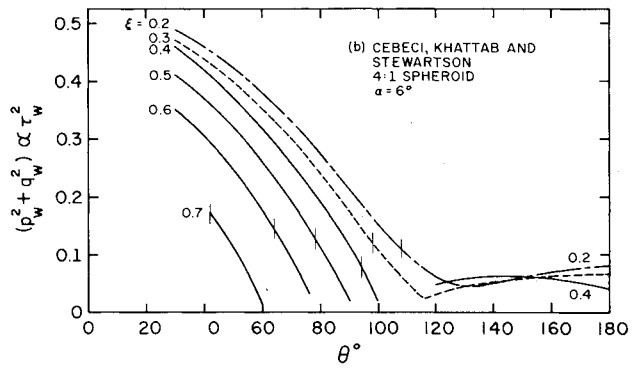

b) Cebeci et al. 4:1 spheroid, $\alpha = 6$ deg.

Fig. 12 Transverse variation of C_f^2.

the data. In order to explore the detailed behavior of the calculations, Fig. 12a shows the variation of C_f^2. The recent results of Cebeci et al.[18] for a 4:1 spheroid at $\alpha = 6$ deg are presented in the same format in Fig. 12b to show the remarkable similarity between the two sets of calculations for different spheroids and incidences.

It is evident from Figs. 11 and 12a that, in the present case, the resultant wall shear stress approaches zero, within the uncertainties of numerical analysis, at $X/L = 0.4$ and $\theta \sim 122$ deg. In fact, Fig. 12a shows that C_f vanishes as the square root of the distance from this point from both sides but at different rates, suggesting the presence of a Goldstein type of singularity (see Ref. 18). Thus, it is not surprising that numerical difficulties are first encountered there. It is reasonable to infer that this is the most upstream point on the separation line as predicted by boundary-layer theory, regardless of how that line is defined or the shape it takes further downstream.

The solutions downstream of $X/L = 0.4$ are quite well behaved, are grid-independent on the windward side, and show a very rapid decrease in the wall shear-stress magnitude to the leeside of the CFR line. It is tempting to infer, by very short extrapolations from the windward side, that the predicted shear stress vanishes along some line lying a short distance to the lee of the CFR line. Although this would provide an unambiguous definition of separation, the numerical evidence is not conclusive since grid-independent solutions could not be obtained beyond the CFR line. Furthermore, such a definition also would not be general enough to encompass certain special cases, such as the separation on an infinite swept wing. However, the present solutions, like those of Cebeci et al.[18] and others, indicate a singular behavior in the boundary-layer equations; consequently we conclude that it is not possible to determine the flow properties along the line of separation from boundary-layer equations alone, regardless of the numerical scheme used to approach the separation line. Second, the present controversy[24] concerning the shape of the separation line, i.e., whether it is closed or open, can not be settled on the basis of boundary-layer calculations.

V. Conclusions

The calculations of the laminar boundary layer on a 6:1 spheroid at an incidence of 10 deg reproduce many of the features observed in the low Reynolds number experiments of Meier et al.[7-10] The experiments indicate a limited region of transitional or turbulent flow, but no attempt has been made here to model this part of the flow.

The laminar-flow calculations break down in a wedge-shaped region that starts at a point where the predicted wall shear stress vanishes. This region coincides roughly with the observed zone of transitional and turbulent flow. The solution features indicate a singular behavior of the boundary-layer equations along a line that emanates from the point of zero predicted stress and coincides with the line along which the measured stress became very small. This line lies a short distance to the leeward side of the line of circumferential flow reversal, which is well defined and can be predicted with accuracy. The singularity in the equations precludes any conclusions concerning the location, origin, and shape of the separation line on the basis of boundary-layer theory. Solutions with higher order equations and strong viscous-inviscid interactions are therefore required to resolve the controversy regarding the occurrence of closed or open separation lines on bodies at different incidences.

The solutions at the higher Reynolds number indicate that they are quite successful in predicting the observed characteristics of the boundary layer over a large part of the body where the boundary layer is thin. Some modifications of the turbulence model are needed to improve the representation of the flow in the neighborhood of transition. The calculations fail to provide an adequate description of the flow in the region on the leeside where the boundary layer becomes thick. This region is quite extensive and well removed from separation.

The calculations using the potential-flow as well as experimental pressure distributions clearly demonstrate the limitations of first-order boundary-layer theory. In particular, it is shown that knowlege of the experimental pressure distribution on the surface does not lead to a dramatic improvement in the prediction of either separation or thick boundary layers. The latter observation is of considerable practical significance since extensive regimes of thick boundary layers may be present on bodies such as aircraft fuselages and ships (Patel[25]) without encountering separation. Once again, the results presented here suggest that such flows can be calculated only by recourse to higher order equations that allow for the viscous-inviscid interaction through the relaxation of the pressure field.

Acknowledgments

This research has been supported by the U.S. Army Research Office and the U.S. Air Force Office of Scientific Research under Grant AFOSR-80-0148-B. The authors also acknowledge the timely assistance of Dr. A.W. Fiore of the AFFDL and Dr. H.U. Meier of the DFVLR, Project Officers of the United States and Federal Republic of Germany Data Exchange Agreement, in making available the data from the DFVLR experiments.

References

[1] Werle, H., "Separation on Axisymmetrical Bodies at Low Speed," *Rech. Aeron.*, No. 90, 1962, pp. 3-14.

[2] Wilson, G.R., "Experimental Study of Laminar Boundary Layer on a Body of Revolution," M.Sc. Thesis, Air Force Institute of Technology, WPAFB, GAM/AE/71-4, 1971.

[3] Peake, D.J., Rainbird, W.J., and Atraghji, E.G., "Three-Dimensional Flow Separation on Aircraft and Missiles," *AIAA Journal*, Vol. 10, May 1972, pp. 567-580.

[4] Han, T.-Y. and Patel, V.C., "Flow Separation on a Spheroid at Incidence," *Journal of Fluid Mechanics*, Vol. 92, 1979, pp. 643-657.

[5] Ramaprian, B.R, Patel, V.C., and Choi, D.H., "Mean Flow Measurements in the Three-Dimensional Boundary Layer over a Body of Revolution at Incidence," *Journal of Fluid Mechanics*, Vol. 103, 1981, pp. 479-504.

[6] Hayashita, S., "Flow Around a Spheroid at Angle of Attack," *Transactions of the Society of Naval Architects of West Japan*, Vol. 63, No. 2, 1981, pp. 41-50.

[7] Meier, H.U. and Kreplin, H.P., "Experimental Investigations of Boundary Layer Transition and Separation on a Body of Revolution," *Zeitschrift für Flugwissenschaft Weltraumforschung*, Vol. 4, 1980, pp. 65-71.

[8] Meier, H.U. and Kreplin, H.P., "Experimental Study of Boundary Layer Velocity Profiles on a Prolate Spheroid at Low Incidence in the Cross-Section $X/L = 0.64$," *Proceedings of 5th USAF-FRG Data Exchange Agreement Meeting*, AFFDL-TR-80-3088, 1980, pp. 169-189.

[9] Meier, H.U. Kreplin, H.P., and Vollmers, H., "Velocity Distributions in 3-D Boundary Layers and Vortex Flows on an Inclined Prolate Spheroid," *Proceedings of 6th USAF-FRG Data Exchange Agreement Meeting*, DFVLR-AVA Rept. IB 22281 CPl, 1981, pp. 202-217.

[10] Kreplin, H.P., Vollmers, H., and Meier, H.U., "Measurements of the Wall Shear Stress on an Inclined Prolate Spheroid," *Zeitschrift für Flugwissenschaft Weltraumforschung*, Vol. 6, 1982, pp. 248-252.

[11] Wang, K.C., "Separation Patterns of Boundary Layer Separation over an Inclined Body of Revolution," *AIAA Journal*, Vol. 10, 1972, pp. 1044-1050.

[12] Wang, K.C., "Boundary Layer over a Blunt Body at High Incidence with an Open-Type of Separation," *Proceedings of the Royal Society*, Vol. A340, 1974, pp. 33-55.

[13] Wang, K.C., "Boundary Layer over a Blunt Body at Low Incidence with Circumferential Reversed Flow," *Journal of Fluid Mechanics*, Vol. 72, 1975, pp. 49-65.

[14] Geissler, W., "Three-Dimensional Laminar Boundary Layer over a Body of Revolution at Incidence and with Separation," *AIAA Journal*, Vol. 12, Dec. 1974, pp. 1743-45.

[15] Patel, V.C. and Choi, D.H., "Calculation of Three-Dimensional Laminar and Turbulent Boundary Layers on Bodies of Revolution at Incidence," *Turbulent Shear Flows II*, edited by L.J.S. Bradbury, F. Durst, B.E. Launder, F.W. Schmidt, and J.H. Whitelaw, (Springer-Verlag, New York), 1980, pp. 199-217.

[16] Cebeci, T., Khattab, A.K., and Stewartson, K., "Prediction of Three-Dimensional Laminar and Turbulent Boundary Layers on Bodies of Revolution at High Angles of Attack," *Turbulent Shear Flows II*, edited by L.J.S. Bradbury, F. Durst, B.E. Launder, F.W. Schmidt, and J.H. Whitelaw, Springer-Verlag, New York, 1980, pp. 189-198.

[17] Cebeci, T., Khattab, A.K., and Stewartson, K., "Studies on Three-Dimensional Laminar and Turbulent Boundary Layers on Bodies of Revolution at Incidence. I. Nose Separation," AIAA Paper 79-0138, Jan. 1979.

[18] Cebeci. T., Khattab, A.K., and Stewartson, K., "Three-Dimensional Laminar Boundary Layers and the OK of Accessibility," *Journal of Fluid Mechanics*, Vol. 107, 1981, pp. 57-87.

[19] Stock, H.W., "Laminar Boundary Layers on Inclined Ellipsoids of Revolution," *Zeitschrift für Flugwissenschaft Weltraumforschung*, Vol. 4, 1980, pp. 217-224.

[20] Schneider, G.R., "Calculation of Three-Dimensional Boundary Layers on Bodies of Revolution at Incidence," *Proceedings of 5th USAF/FRG Data Exchange Agreement Meeting*, AFFDL-TR-80-3088, 1980, pp. 287-305.

[21] Ragab, S.A., "A Method for the Calculation of Three-Dimensional Boundary Layers with Circumferential Reversed Flow on Bodies," AIAA Paper 82-1023, 1982.

[22] Patel, V.C. and Baek, J.H., "Calculation of Three-Dimensional Boundary Layers on Bodies at Incidence," Iowa Institute of Hydraulic Research, Rept. 256, 1982.

[23] Nash, J.F. and Scruggs, R.M., "An Implicit Method for the Calculation of Three-Dimensional Boundary Layers on Fuselage Configurations," Sybucon Inc., Atlanta, Ga., Rept. LG76ER0199, 1976.

[24] Wang, K.C., "New Developments About Open Separation," San Diego State University, Rept. AE&FM TR-82-02, 1982.

[25] Patel, V.C., "Some Aspects of Thick Three-Dimensional Boundary Layers," *Proceedings of 14th Symposium on Naval Hydrodynamics*, Ann Arbor, Mich., Aug. 1982, pp. 999-1040.